RESEARCH ARTICLE | JUNE 01 2024

Development of a double-well potential upon collisional activation that facilitates proton transfer in 9-methyl-8-oxoguanine-9-methyladenine base-pair radical cation† ⊘

May Myat Moe; Jianbo Liu ✉

Check for updates

View Online

Export Citation

ARTICLE

Development of a Double-Well Potential upon Collisional Activation that Facilitates Proton Transfer in 9-Methyl-8-oxoguanine–9-Methyladenine Base-Pair Radical Cation[†]

May Myat Moe[a,b], Jianbo Liu[a,b*]

a. Department of Chemistry and Biochemistry, Queens College of the City University of New York, NY 11367, USA
b. The Ph.D. Program in Chemistry, the Graduate Center of the City University of New York, NY 10016, USA

8-Oxoguanine (OG) is the most common oxidatively generated nucleobase damage and can mispair with adenine (A) in Hoogsteen mode during replication. Besides introducing the $G \cdot C \rightarrow T \cdot A$ transversion mutation, the $OG \cdot A$ base pair is vulnerable to ionizing radiation and one-electron oxidation owing to the lower ionization and oxidation potentials of OG than natural DNA nucleobases. Herein, we report the formation and collision-induced dissociation (CID) of the radical cation of a model base pair consisting of nucleoside-mimicking 9-methyl-8-oxoguanine (9MOG) and 9-methyladenine (9MA). The $[9MOG \cdot 9MA]^{•+}$ radical cation is formed in the gas phase by redox-separation of electrospray ionization-produced Cu^{II}-nucleobase complexes, and its CID is examined using guided-ion beam tandem mass spectrometry. Measurement included kinetic energy-dependent dissociation product ions and cross sections, from which the product pairs of $[9MOG − H]^{•} + [9MA+H]^{+}$ (major dissociation channel) and $9MOG^{•+} + 9MA$ (minor) were detected with 0 K dissociation threshold energies of 1.8 and 1.65 eV, respectively. The $[9MOG \cdot 9MA]^{•+}$ structures were examined using density functional theory, and important conformations were all featured by complete intra-base pair proton transfer as $[9MOG − H]^{•} \cdot [9MA+H]^{+}$. On the other hand, the production of $9MOG^{•+}+9MA$ in dissociation required a $9MOG^{•+} \cdot 9MA$ intermediate. The results were rationalized by the discovery of a double-well potential that evolves on the reaction potential energy surface of the collisionally activated base pair, leading to the proton-transfer equilibrium of excited $([9MOG − H]^{•} \cdot [9MA+H]^{+})^{*} \rightleftharpoons (9MOG^{•+} \cdot 9MA)^{*}$. The combined experimental and theoretical work provides insight into the less intuitive aspects of this biologically-important, non-canonical base pair, especially its opening upon oxidative and ionization damage.

Key words: Base-pair radical cation, Collision-induced dissociation, Intra-base pair proton transfer, Reaction potential energy surface, Electrospray ionization mass spectrometry, Guided-ion beam scattering
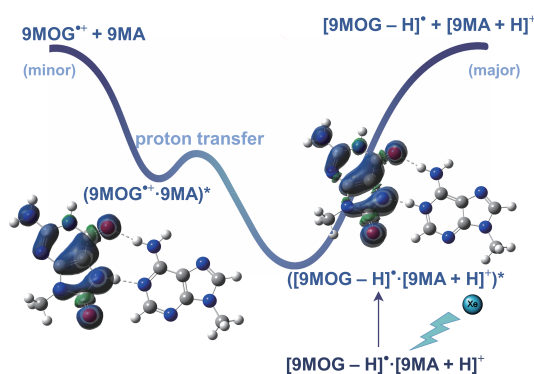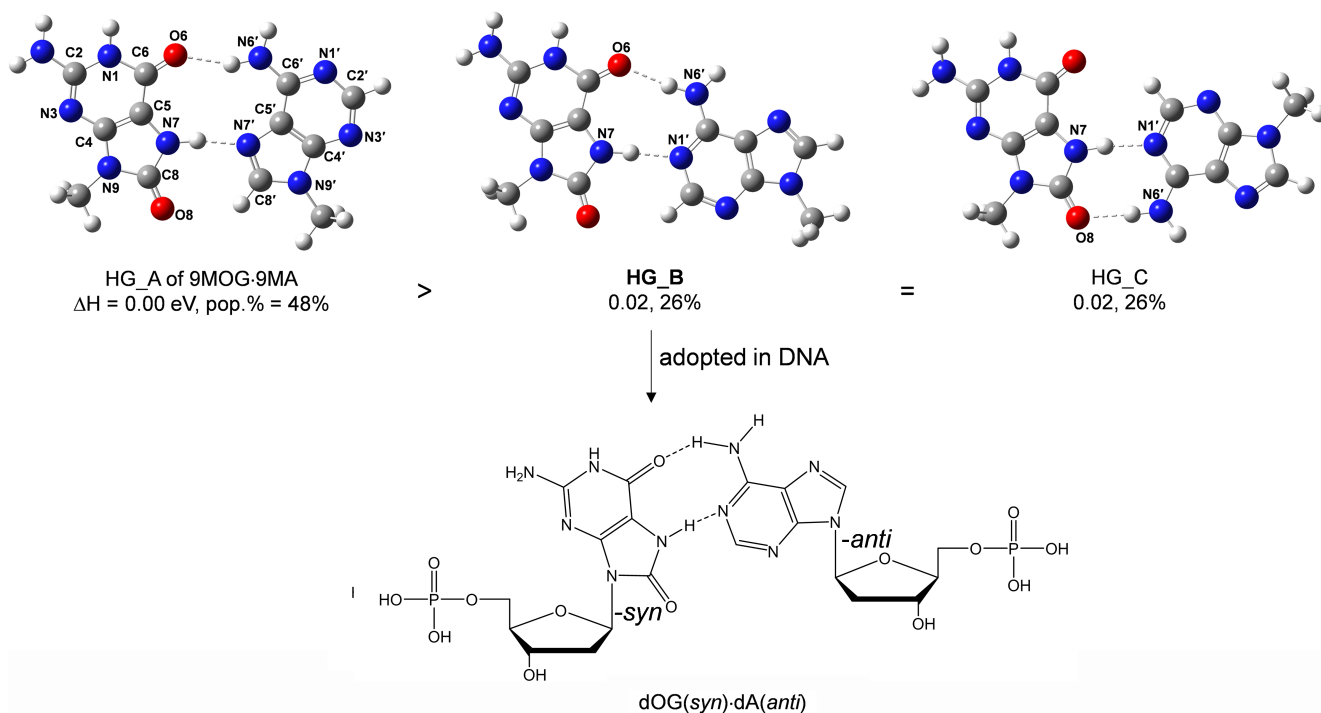
I. INTRODUCTION

Guanine (G), due to its lowest adiabatic ionization potential (AIP = 7.68 eV [1, 2]) and oxidation potential

Scheme 1. Various Hoogsteen conformers of neutral 9MOG·9MA with atomic numbering. Dashed lines indicate H-bonds. Relative formation enthalpies (ΔH with respect to HG_A) and Boltzmann populations were calculated at 298 K using the ωB97XD/6-311++G(d,p) level of theory, including thermal corrections. Shown at the bottom is the conformation of dOG(*syn*)·dA(*anti*) in DNA.

(E° *vs.* NHE = 1.29 V [3, 4]) among the natural DNA components (*i.e.*, nucleobase, deoxyribose, and phosphate), represents the most oxidizable DNA target upon the attack of ionizing radiation and exogenous and endogenous oxidants. The oxidative damage of guanine is reflected in a wide variety of genotoxic lesions, including the formation of 8-oxoguanine (OG) [5, 6], spiroiminodihydantoin (Sp) [7−10], guanidinohydantoin (Gh) [7, 9], 2,5-diaminoimidazolone (Iz) [11, 12], 2,2,4-triamino-2H-oxazol-5-one (Oz) [11−13], and 2,6-diamino-4-hydroxy-5-formamidopyrimidine (FapyG) [12, 14, 15]. Among these, OG is the most common and being used as a biomarker of oxidative stress in cells and tissues [16, 17]. Notably, OG is even more prone to ionization and oxidation due to its AIP and E° being 0.75 eV [18] and 0.55 eV [19] lower than those of guanine, respectively. These lead to the facile formation of the OG radical cations (OG$^{\bullet+}$) upon ionizing radiation, one-electron oxidation, type I photo-oxidation, *etc.*

OG has high mutagenicity, because it prefers to form a mismatched Hoogsteen (HG) base pair with adenine (A) instead of a correct Waston-Crick (WC) base pair with cytosine (C) during cellular DNA replication [20−26]. Scheme 1 shows probable HG-type OG·A con-

formers consisting of 9-methyl-8-oxoguanine (9MOG) and 9-methyladenine (9MA), in which the methyl groups mimic the nucleoside sugar moieties. These structures were optimized using density functional theory (DFT) at the ωB97XD/6-311++G(d,p) level of theory. In the lowest-energy conformer HG_A, the O6 and N7−H at the HG edge of 9MOG engage in hydrogen bonding with the N6'−H and N7' at the HG edge of 9MA, respectively. The conformers HG_B and HG_C have the same energy. In HG_B, the O6 and N7−H of 9MOG are hydrogen bonded to the N6' and N1' at the WC edge of 9MA. In HG_C, the intra-base pair hydrogen bonds consist of (9MOG)N7−H···N1'(9MA) and (9MOG)O8···H−N6'(9MA). As characterized by the NMR [21, 27] and X-ray crystallographic structure [23, 25, 28] of DNA containing an 8-oxo-2'-deoxyguanosine (dOG)·2'-deoxyadenosine (dA) base pair, dOG adopts a *syn*-conformation around the N9-glycosidic bond to avoid steric repulsion between the O8 and the sugar phosphate backbone (for comparison, an unmodified 2'-deoxyguanosine adopts an *anti*-conformation). The *syn*-glycosidic torsion allows the HG edge of OG hydrogen bonded to the WC edge of dA in an *anti*-glycosidic conformation on the complementary strand, as illustrated

by the Chemdraw schematic in Scheme 1. It follows that only HG_B represents the dOG·dA in DNA. The preference of HG_B over HG_A and C in DNA is supported by several factors. First, replacing adenine with 7-deaza-adenine (*i.e.*, deazaA, replacing the N7 of adenine with a -CH) had no influence on the polymerase X synthesis efficiency of OG·deazaA, suggesting that the (OG)N7−H···N7'(A) hydrogen bond is not important [29]. Secondly, the conformation HG_C would force dA to change from the standard *anti*-orientation to *syn* with only one effective hydrogen bond with dOG(*syn*) [30, 31]. Last yet biologically most significant, there is a structural similarity between HG_B and a cognate T(thymidine)·A base pair both in the minor groove and in the backbone region [22, 24, 28]. Therefore, HG_B is able to evade error detection by not distorting the polymerase active site [32]. Consequently, this mismatch cannot be efficiently processed by the human mismatch repair system and ultimately leads to the G·C→T·A transversion mutation [25, 33]. The latter represents the second most frequent somatic mutation found in human cancers [33, 34].

As mentioned above, OG has a lower $E°$ than all other DNA nucleobases and thus serves as a trap for radical cations in an oxidized DNA helix. Related to this, it was reported that the OG·A mispair is 2.5 times more reactive toward oxidation than the OG·C base pair [35]. According to the B3LYP/6-311G(d,p) calculations reported by Reynisson and Steenken [26], the one-electron oxidation of OG·A in a HG_B conformation leads to a complete proton shift from the N7−H of $OG^{•+}$ to the N1' of A. The resulting $[OG − H_{N7}]^{•} \cdot [A+H_{N1'}]^{+}$ structure has a binding energy higher than that of the classical Waston-Crick G·C by 37 kJ/mol; for comparison, the neutral OG·A has a binding energy lower than that of G·C by 59 kJ/mol [26]. Therefore, the ionization accompanied with intra-base pair proton transfer (PT) introduces not only structural changes but also energetic perturbations in OG·A, all of which warrant experimental study. The experimental study will also help understand the Löwdin spontaneous point mutation mechanism [36] and charge transfer along the DNA helix [37]. Surprisingly, the experimental investigation of $[OG·A]^{•+}$ appears to be sparse. To the best of our knowledge, the present work represents the first of its kind. In this work, the base-pair binding energy was examined using collision-induced dissociation (CID). CID results provided not only quantitative measures of base-

pairing strength but also the insight into the PT dynamics, as a proton-transferred base-pair structure would produce a distinctly different product pair from that of a conventional base-pair structure.

The remaining parts of the paper are organized as follows. Instrumentation, experimental and data analysis methods for the formation and CID of a model base pair $[9MOG·9MA]^{•+}$, as well as quantum chemistry computational approaches, are described in Section II. The results of kinetic energy-dependent base-pair CID are reported in Section III, followed by identification of base-pair structures and determination of dissociation threshold energies for individual product channels. The reaction potential energy surfaces (PESs) for the collisionally activated base pairs are modeled in Section IV, focusing on the consequences of base-pair excitation on intra-base pair PT. Finally, conclusions are presented in Section V.

II. METHODS

A. CID experiment

The CID experiment was carried out on a home-built guided-ion beam tandem mass spectrometer coupled to an electrospray ionization (ESI) ion source. Details of the instrumentation, operation and calibration are available in the previous report [38]. In brief, the apparatus consists of a radio-frequency (rf) hexapole ion guide, a reactant quadrupole mass filter, a rf octopole ion guide, a product quadrupole mass filter, and a pulse-counting ion detector. The $[9MOG·9MA]^{•+}$ radical cations were produced by redox dissociation of Cu^{II}-nucleobase complexes [39, 40]. The similar procedure was used for generating $[G·C]^{•+}$ [41], $[G·G]^{•+}$ [39, 42], $[OG·G]^{•+}$ [39, 42], and $[OG·C]^{•+}$ [43] base-pair radical cations. A methanol/water ($v{:}v = 3{:}1$) solution containing a mixture of 0.5 mmol/L 9MOG (synthesized at University of Konstanz, Germany) [44], 0.5 mmol/L 9MA (Acros, 98%), and 0.25 mmol/L Cu(NO₃)₂ (Alfa Aesar, 99.999%) was electrosprayed into the ambient atmosphere at a 0.06 mL/h flow rate. The $[Cu^{II}(9MOG)_m(9MA)_n]^{•2+}$ complexes formed in the electrospray were introduced into the mass spectrometer through a heated (190 °C) desolvation capillary. The source chamber (maintained at a pressure of 1.6 Torr) of the mass spectrometer is separated from the hexapole ion guide (at a pressure of 10−20 mTorr) by a skimmer located at 3 mm away from the end of the

capillary. The capillary and the skimmer were each biased at 76 V and 18 V, and the electric field between the two promoted CID of the Cu^{II}-base pair complexes with the background gas, including the redox dissociation of $[Cu^{II}(9MOG\cdot9MA)_3]^{\bullet2+} \rightarrow [Cu^{I}(9MOG\cdot9MA)_2]^{+} + [9MOG\cdot9MA]^{\bullet+}$ [39, 40]. The ion intensity of $[9MOG\cdot9MA]^{\bullet+}$ was 2×10^3 counts/s.

Ions including $[9MOG\cdot9MA]^{\bullet+}$ were transported to the hexapole ion guide, where they were collisionally focused to a well-defined kinetic energy (with an average value equal to the hexapole DC bias potential) and thermalized to Maxwell-Boltzmann vibrational (E_{vib}) and rotational (E_{rot}) energy distributions at 310 K [38]. The previous measurements of the dissociation threshold energies for the base-pair radical cations containing $9MOG^{\bullet+}$ [42, 43] and/or $9MG^{\bullet+}$ [41] confirmed that these nucleobases adopted the lowest-energy O6-keto tautomer in the ion beam, presumably because all reactant structures (and any high-energy tautomers if formed) had been relaxed to the thermal equilibrium populations.

The $[9MOG\cdot9MA]^{\bullet+}$ radical ions were selected by the reactant quadrupole mass filter and subsequently injected into the octopole ion guide. The octopole was driven by a combination of DC and rf potentials, which decelerated/accelerated reactant ions to a desired kinetic energy in the laboratory frame (E_{lab}) and guided the ions through an 11-cm long scattering cell filled with the Xe target gas. The absolute zero point and full width at half-maximum (FWHM) of E_{lab} were determined by scanning the octopole DC potential, *i.e.*, a retarding potential measurement [38, 45]. E_{lab} was converted to the collision energy (E_{CM}) in the center-of-mass frame by $E_{CM} = E_{lab} \times m_{neutral}/(m_{neutral}+m_{ion})$, where $m_{neutral}$ and m_{ion} are the masses of the neutral and ionic reactants, respectively. The uncertainty of absolute E_{lab} was <0.1 eV and its FWHM was 0.65 eV. These corresponded to an uncertainty of <0.03 eV and a FWHM of 0.18 eV in the E_{CM} for $[9MOG\cdot9MA]^{\bullet+} +$ Xe. Product ions and remaining reactant ions were analyzed by the product quadrupole mass filter and counted.

The Xe pressure within the scattering cell was maintained at 0.015 mTorr. At this gas pressure, the probability for single ion–Xe collisions was 3%, and that for double collisions or more was $<0.1\%$. The thin-target condition allowed product ion cross sections to be calculated using the Beer-Lambert law [46, 47]. The background ion intensities (when the Xe gas was no longer

directed into the scattering cell) were corrected in the measurement.

B.   Analysis of dissociation threshold energy

A modified line-of-centers (LOC) model [46, 48–50] was used to fit the kinetic energy dependence of the CID cross section. The model assumes that a fraction of near-threshold collisions may contribute all of the energy to overcome E_0 (*i.e.*, completely inelastic) as described by Eq.(1) [46, 50, 51]:

$$\sigma(E) = \sigma_0 \frac{(E_{CM} + E_{vib} + E_{rot} - E_0)^n}{E_{CM}} \qquad (1)$$
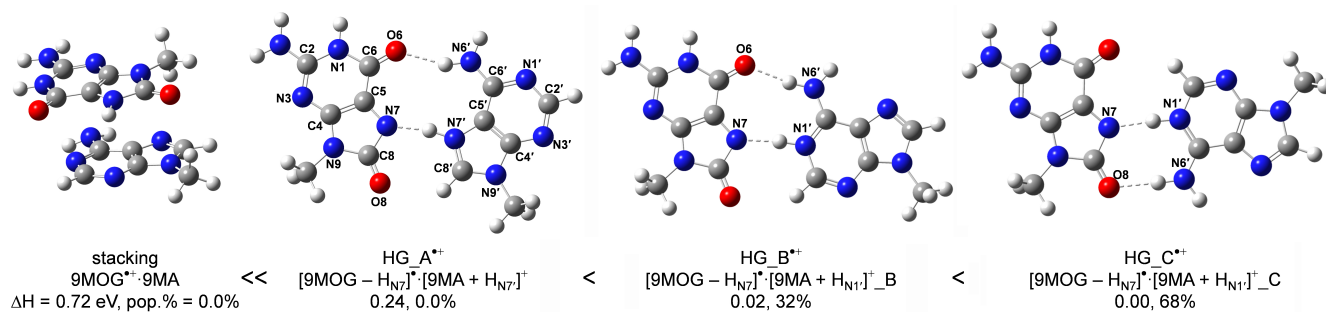
where σ_0 is a scaling factor, E_{CM}, E_{vib}, and E_{rot} are as described before, E_0 is the dissociation threshold energy at 0 K, and n is a fitting parameter that determines the energy transfer efficiency from E_{CM} to the base-pair internal energy.

The energy dependence of $\sigma(E)$ was broadened by reactant internal and kinetic energy distributions [52, 53]. To mimic energy broadening in the $\sigma(E)$ fitting, a Monte Carlo program [41, 54] was used to simulate the ion–Xe collisions. 100000 collisions were simulated for each product ion channel and at each E_{CM}. In the collisions, the $[9MOG\cdot9MA]^{\bullet+}$ ions were sampling E_{vib} and E_{rot} at 310 K, and E_{lab} (corresponding to the desired E_{CM}) with a FWHM of 0.65 eV, while the Xe atoms were sampling the kinetic energy distribution at room temperature. The simulation results were used for the convolution of Eq.(1) over energy broadening.

In addition, each collision that had total energy exceeding E_0 was subjected to the kinetic shift [55] analysis using the Rice-Ramsperger-Kassel-Marcus (RRKM) theory [56]. Only the collisions that had led to a dissociation within the ion time-of-flight (100−500 μs) were counted toward $\sigma(E)$. The values of E_0 and n were adjusted until the convoluted $\sigma(E)$ matched the experiment, and a leveling-off function was used to allow $\sigma(E)$ to reach a plateau at high E_{CM}.

C.   Computations

Electronic structure and PES calculations were performed using the Gaussian 16 program suite [57]. Structures of nucleobases and base pairs were optimized using the ωB97XD/6-311++G(d,p) method to mitigate self-interaction errors of radical cations [58]. The relaxed PESs were constructed at the ωB97XD/6-31+G(d,p) level of theory based on the consideration of

02 June 2024 19:27:07

stacking		HG_A$^{\bullet+}$		HG_B$^{\bullet+}$		HG_C$^{\bullet+}$
9MOG$^{\bullet+}$·9MA	$\ll$	[9MOG − H$_{N7}$]$^{\bullet}$·[9MA + H$_{N7}$]$^+$	$<$	[9MOG − H$_{N7}$]$^{\bullet}$·[9MA + H$_{N1'}$]$^+$_B	$<$	[9MOG − H$_{N7}$]$^{\bullet}$·[9MA + H$_{N1'}$]$^+$_C
ΔH = 0.72 eV, pop.% = 0.0%		0.24, 0.0%		0.02, 32%		0.00, 68%

Scheme 2. Various conformers of [9MOG·9MA]$^{\bullet+}$ with atomic numbering. Dashed lines indicate H-bonds. Relative enthalpies (ΔH with respect to HG_C$^{\bullet+}$) and Boltzmann populations were calculated at 298 K using the ωB97XD/6-311++G(d,p) level of theory, including thermal corrections.

both computational cost and accuracy, and all bond lengths and angles were optimized at each grid point except the scanning coordinates. Zero-point energies (ZPEs, scaled by a factor 0.975 [59]) and basis set superposition errors (BSSEs, estimated using the counterpoise calculations [60]) were all corrected in the calculations of dissociation threshold energies.

III. EXPERIMENTAL RESULTS

A. DFT-calculated structures of [9MOG·9MA]$^{\bullet+}$

Consistent with the report of Reynisson and Steenken [26], the N7−proton of 9MOG$^{\bullet+}$ in [9MOG·9MA]$^{\bullet+}$ is completely shifted to 9MA, rendering the formation of a proton-transferred structure from each of the neutral HG_A, HG_B, and HG_C. The resulting ionic conformers are presented in Scheme 2, and referred to as HG_A$^{\bullet+}$ (in a [9MOG − H$_{N7}$]$^{\bullet}$·[9MA+H$_{N7}$]$^+$ structure), HG_B$^{\bullet+}$ and HG_C$^{\bullet+}$ (both has a [9MOG − H$_{N7}$]$^{\bullet}$·[9MA +H$_{N1'}$]$^+$-like structure), respectively. In addition, a stacking base pair structure was identified.

The fact that there are no conventional conformers (*i.e.*, without intra-base pair PT) for [9MOG·9MA]$^{\bullet+}$ is distinctively different from many other singly charged base pairs, such as the protonated [51, 61], deprotonated [62], and radical cationic [41−43] G·C and OG·C base pairs. In the latter, conventional and proton-transferred structures co-exist at ground state. The discrepancy is not surprising given that the large difference in the following pK_a values: pK_a = 0.23 for 9MOG$^{\bullet+}$ (N7−H) [63], 4.1 for 9MA (N1) [64], and 3.51 for 9MA (N7) [65].

Hydrogen transfer from the N6'−H of 9MA to the O6 or O8 of 9MOG is possible, but the resulting conformers (see HG_D$^{\bullet+}$, E$^{\bullet+}$ and F$^{\bullet+}$ in Scheme S1 of Supplementary materials, SM) all have energies higher than

the global minimum conformer by more than 1.2 eV, ruling out their participations in the experiment. This is consistent with the experimental results to be described below— that is no [9MOG +H]$^+$ was observed in the CID products. In sum, our computation not only reproduced the previously reported HG_B$^{\bullet+}$ structure [26] but also discovered the new HG_A$^{\bullet+}$, HG_C$^{\bullet+}$, and the stacking structure.

Also consistence with the previous report [26] is that the ionization of 9MOG increases the base-pair binding energy. The 0 K binding energies are 0.70 eV (67.5 kJ/mol), 0.68 eV (65.6 kJ/mol), and 0.68 eV (65.6 kJ/mol) for the neutral HG_A, HG_B, and HG_C, respectively; and increase to 1.63 eV (157.3 kJ/mol), 1.85 eV (178.5 kJ/mol), 1.86 eV (179.5 kJ/mol), and 0.93 eV (89.7 kJ/mol) for HG_A$^{\bullet+}$, HG_B$^{\bullet+}$, HG_C$^{\bullet+}$, and the stacking 9MOG$^{\bullet+}$·9MA, respectively. The amount of increase from HG_A, HG_B, and HG_C to their ionized counterparts ranges from 0.93 eV to 1.18 eV. On the other hand, the hydrogen bond lengths in these conformers only vary by −0.06 Å to +0.07 Å upon ionization—an extent that is not sufficiently large to bring about a dramatic increase in binding energy. Therefore, the enhanced binding energy is most likely attributed to the enhanced ion-dipole interaction arising from the PT-induced spin-charge separation.

The ionization and accompanying PT have reversed the relative stabilities among different base-pair conformers. According to Boltzmann populations in Scheme 2, only HG_B$^{\bullet+}$ and HG_C$^{\bullet+}$ were expected to make significant contributions in the reaction. These two conformers were lumped as [9MOG − H$_{N7}$]$^{\bullet}$·[9MA +H$_{N1'}$]$^+$ in the analyses of CID results. When there is a need to distinguish individual conformations, suffixes B and C are added to the structural formula.
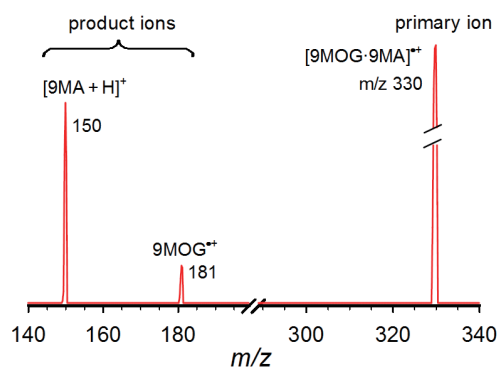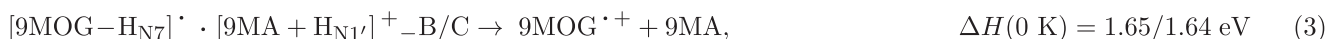
02 June 2024 19:27:07

FIG. 1 CID product ion mass spectrum of $[9MOG - H_{N7}]^{\bullet} \cdot [9MA + H_{N1'}]^{+}$ recorded at $E_{CM} = 3.0$ eV.

B. CID product ions and cross sections

CID product ions of $[9MOG - H_{N7}]^{\bullet} \cdot [9MA + H_{N1'}]^{+}$ were measured over an E_{CM} range from 0.05 eV to 5.0 eV. A representative product ion mass spectrum, measured at $E_{CM} = 3.0$ eV, is presented in FIG. 1. CID product ions include not only $[9MA + H]^{+}$ (m/z 150) but also $9MOG^{\bullet+}$ (m/z 181). $[9MA + H]^{+}$ is what we had expected from the CID of $[9MOG - H_{N7}]^{\bullet} \cdot [9MA + H_{N1'}]^{+}$, but production of $9MOG^{\bullet+}$ would not be possible unless there was back proton transfer in $[9MOG - H_{N7}]^{\bullet} \cdot [9MA + H_{N1'}]^{+}$ upon collision activation.

Since product ions were produced from a mixture of $[9MOG - H_{N7}]^{\bullet} \cdot [9MA + H_{N1'}]^{+}\_B$ and $[9MOG - H_{N7}]^{\bullet} \cdot [9MA + H_{N1'}]^{+}\_C$, the $\Delta H(0\ \text{K})$ for each product channel was calculated for individual starting structures at the ωB97XD/6-311++G(d,p) level of theory and are listed below:

$$[9MOG - H_{N7}]^{\bullet} \cdot [9MA + H_{N1'}]^{+}\_B/C \rightarrow [9MOG - H_{N7}]^{\bullet} + [9MA + H_{N1}]^{+}, \qquad \Delta H(0\ \text{K}) = 1.86/1.85\ \text{eV} \quad (2)$$

$$[9MOG - H_{N7}]^{\bullet} \cdot [9MA + H_{N1'}]^{+}\_B/C \rightarrow 9MOG^{\bullet+} + 9MA, \qquad \Delta H(0\ \text{K}) = 1.65/1.64\ \text{eV} \quad (3)$$

Cross sections for individual product ions are presented in FIG. 2, wherein error bars represent standard deviations determined from four sets of measurements. The sum of product ion cross sections reaches a plateau of 150 Å^2 at E_{CM} above than 3 eV. This value is close to the collision cross section of the base pair with Xe estimated using the IMoS program [66, 67]. There is no obvious inflection in either of the two product ion cross sections in the near-threshold energy region. This implies that all of the $[9MA + H_{N1}]^{+}$ ions were produced

via the same mechanism and with the same dissociation threshold, and the same is true for $9MOG^{\bullet+}$.

C. Base-pair dissociation threshold energies

The kinetic energy width and the E_{vib} and E_{rot} distributions of the $[9MOG - H_{N7}]^{\bullet} \cdot [9MA + H_{N1'}]^{+}$ ion beam, and the Doppler broadening [52, 53] of the Xe atoms were all factored into the near-threshold cross sections. As a result, the product ion cross section rises
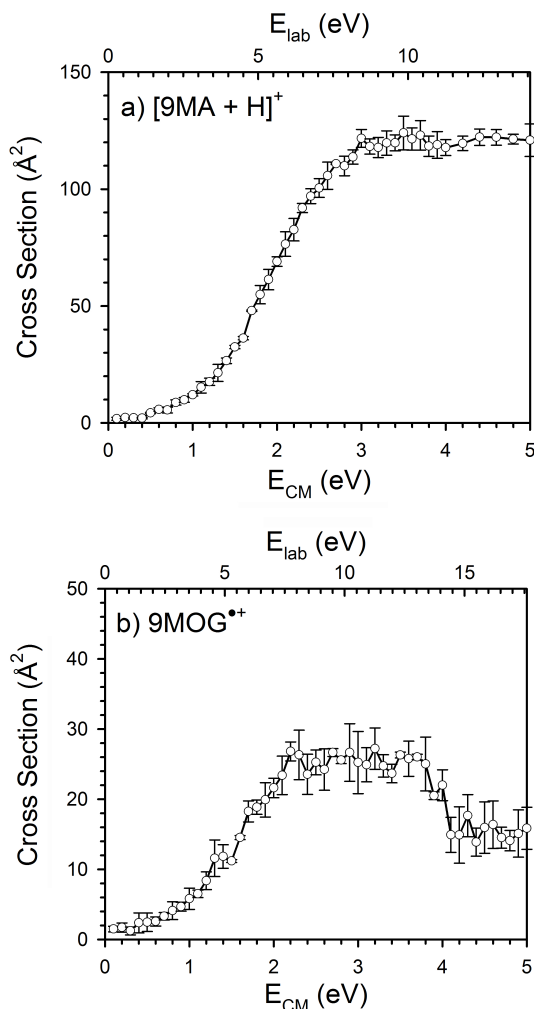

FIG. 2 Product ion cross sections of (a) $[9MA + H]^{+}$ and (b) $9MOG^{\bullet+}$ as a function of kinetic energy in the laboratory frame (E_{lab}, upper x-axis) and center-of-mass frame (E_{CM}, lower x-axis).
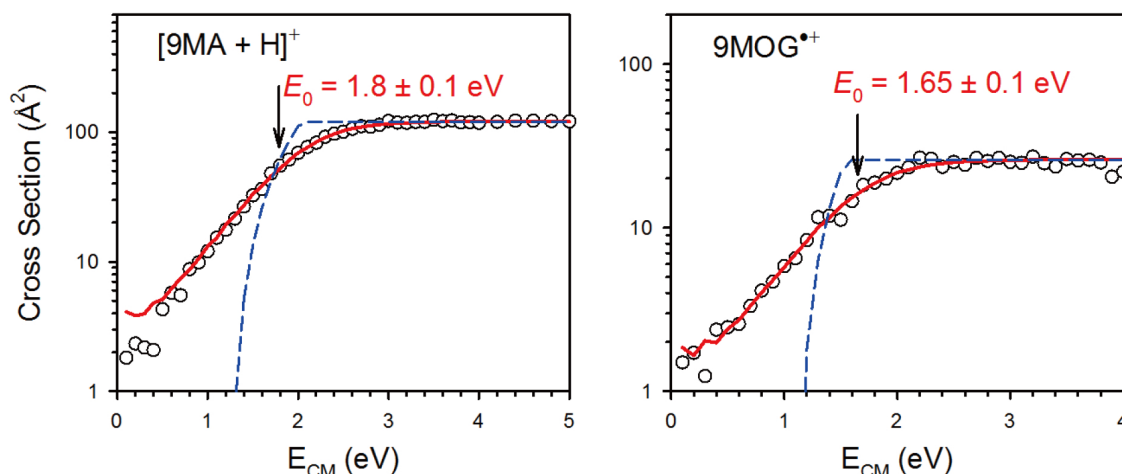
FIG. 3 Extraction of dissociation thresholds using the LOC fitting. In each frame, black circles represent the experimental cross sections, red solid line represents the convoluted LOC cross sections over reactant internal and kinetic energy distributions, and blue dashed line represents the true cross sections in the absence of kinetic energy distributions for reactants.

from zero at E_{CM} lower than the true E_0. To determine the true E_0, the experimental cross sections were analyzed using the LOC model of Eq.(1) to not only include all sources of energy but also convolute with the energy distributions of both reactants.

FIG. 3 shows the LOC fittings for the cross sections of $[9MA+H_{N1}]^+$ and $9MOG^{\bullet+}$ on a logarithmic scale. In the figure, circles represent the actual experimental data, red solid lines represent the LOC fits with the fitted E_0 marked, and blue dashed lines represent the true LOC cross sections in the absence of reactant energy broadening. The LOC model is able to accurately reproduce the product ion cross sections over two orders of magnitude and from an energy below the threshold to 4−5 eV. The uncertainties of E_0 were determined from several independent fits using an acceptable range of n (2.0–2.2) and included the absolute uncertainty in E_{CM}.

On the basis of the LOC fitting, E_0 was determined to be 1.8±0.1 eV for $[9MOG-H]^\bullet + [9MA+H]^+$ and 1.65±0.1 eV for $9MOG^{\bullet+}+9MA$, which exactly matches the DFT-calculated $\Delta H(0K)$ for reactions (2) and (3). Now the questions arise as to how the product pair of $9MOG^{\bullet+} + 9MA$ was produced from a $[9MOG-H_{N7}]^\bullet \cdot [9MA+H_{N1'}]^+$ structure. More explicitly, how the back proton transfer could happen in the base pair.

IV.   THEORETICAL MODELING AND DISCUSSION

According to Scheme 2, the $[9MOG-H]^\bullet \cdot [9MA+H]^+$ structure was overwhelmingly dominating in the reactant ion beam, whereas the stacking $9MOG^{\bullet+}\cdot 9MA$ had
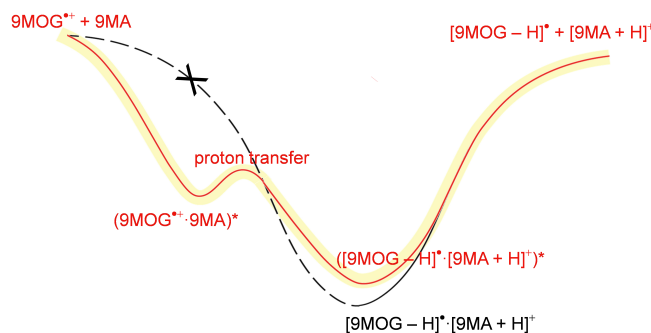
Scheme 3. A double-well potential for $([9MOG - H_{N7}]^\bullet \cdot [9MA+H_{N1'}]^+)^* \rightleftharpoons (9MOG^{\bullet+}\cdot 9MA)^*$, wherein $[9MOG - H_{N7}]^\bullet \cdot [9MA+H_{N1'}]^+$ correlates to the product asymptote $[9MOG - H]^\bullet + [9MA+H]^+$ and $9MOG^{\bullet+}\cdot 9MA$ correlates to the product asymptote $9MOG^{\bullet+} + 9MA$.

negligible thermal population. By directly following the potential energy profile leading from $[9MOG - H]^\bullet \cdot [9MA+H]^+$ (see the black curve in Scheme 3), one would expect only the product asymptote $[9MOG - H]^\bullet+[9MA+H]^+$. On the other hand, the production of the two different product asymptotes required both $[9MOG–H_{N7}]^\bullet \cdot [9MA+H_{N1'}]^+$ and $9MOG^{\bullet+}\cdot 9MA$ as dissociating precursors. Note that the base-pair CID can be viewed as two steps: $[9MOG - H_{N7}]^\bullet \cdot [9MA+H_{N1'}]^+ + Xe \rightarrow [9MOG - H_{N7}]^\bullet \cdot [9MA+H_{N1'}]^+ \cdot Xe$ (a transition collision complex) $\overset{-Xe}{\rightarrow}$ $([9MOG - H_{N7}]^\bullet \cdot [9MA+H_{N1'}]^+)^*$ (a vibrationally excited precursor), followed by intra-base pair vibrational energy redistribution (IVR), and finally separation of the base pair. The "apparent" controversy between the starting base-pair structure and dissociation product structures led us to hypothesize a proton transfer reaction of

$([9MOG - H]^{\bullet} \cdot [9MA+H]^{+})^{*} \rightleftharpoons (9MOG^{\bullet+} \cdot 9MA)^{*}$ during collisional activation. In that case, the dissociation of the activated $[9MOG - H]^{\bullet} \cdot [9MA+H]^{+}$ and $9MOG^{\bullet+} \cdot 9MA$ each correlate to the product asymptotes of $[9MOG - H]^{\bullet} + [9MA+H]^{+}$ and $9MOG^{\bullet+} + 9MA$, respectively, as illustrated by the highlighted surface featured by a double-well potential.

To explore the applicability of the double-well potential model, we turned to mimic the base-pair activation in a relaxed 2D PES scan. The PES in FIG. 4(a) was mapped out along $r(N7–N1')$ (*i.e.*, the distance between the N7 of 9MOG and N1' of 9MA) and $r(N7–H)$ of 9MOG in $[9MOG - H_{N7}]^{\bullet} \cdot [9MA +H_{N1'}]^{+}\_C$. The $r(N7–N1')$ represents the base-pair separation coordinate and thus reflects a direct consequence of collisional activation. The $r(N7–H)$ describes the extent of proton transfer from $9MOG^{\bullet+}$ to 9MA. The PES scanned $r(N7–N1')$ from 2.8 Å to 4.0 Å and $r(N7–H)$ from 0.95 Å to 2.9 Å, with a step size of 0.1 Å for $r(N7–N1')$ and 0.05 Å for $r(N7–H)$. The other molecular structural parameters were all fully optimized at each step. The potential energy was calculated at the ωB97XD/6-31+G(d,p) level of theory and plotted with respect to the electronic energy of a stationary $[9MOG - H_{N7}]^{\bullet} \cdot [9MA +H_{N1'}]^{+}$ without ZPE. To help distinguish potential well and potential ridge, both color-scaled contour map and the values of potential energy are superposed on the 2D surface. The PES presents (1) only one global minimum structure at $r(N7–N1') = 2.8$ Å and $r(N7–H) = 1.75$ Å, which corresponds to the equilibrium structure of $[9MOG - H_{N7}]^{\bullet} \cdot [9MA +H_{N1'}]^{+}\_C$; and (ii) a potential ridge as the surface propagates toward large $r(N7–N1')$, which represents an energy barrier for intra-base pair proton transfer.

FIG. 4(b) provides an alternative display of the PES, wherein a series of slice view is shown at successively increasing $r(N7–N1')$. We can view in FIG. 4(b) how a double-well proton-transfer PES develops during the base-pair dissociation. In the first slice, $r(N7–N1')$ is kept at 2.8 Å (*i.e.*, without stretching the base pair) while $r(N7–H)$ is scanning from 1.05 Å to 2.55 Å, the relaxed PES scan has identified only a single local minimum $[9MOG–H_{N7}]^{\bullet} \cdot [9MA +H_{N1'}]^{+}$ which is located at $r(N7–H) = 1.75$ Å and $r(N1'–H) = 1.05$ Å. The potential becomes increasingly repulsive toward small $r(N7–H)$, indicating there is no stationary $9MOG^{\bullet+} \cdot 9MA$ structure.
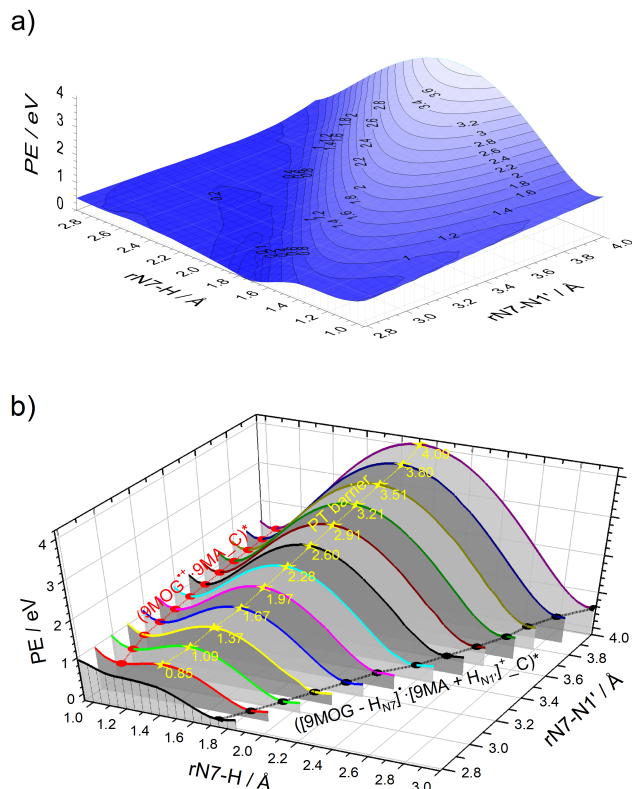
The scenario changes starting from the second slice

FIG. 4 (a) Relaxed 2D PES scan along $r(N7–N1')$ and $r(N7–H)$ for $[9MOG - H_{N7}]^{\bullet} \cdot [9MA+H_{N1'}]^{+}\_C$, calculated at ωB97XD/6-31+G(d,p). Numbers on the contour map are electronic energies with respect to the starting reactant $[9MOG – H_{N7}]^{\bullet} \cdot [9MA+H_{N1'}]^{+}\_C$; and (b) slice view of the PES cutting at different $r(N7–N1')$ values. The evolution of the $9MOG^{\bullet+} \cdot 9MA$ (red dots and trace) $\rightleftharpoons$ $[9MOG - H_{N7}]^{\bullet} \cdot [9MA+H_{N1'}]^{+}$ (black dots and trace) equilibrium is highlighted, with the barrier height for PT indicated for each slice.

when $r(N1'–H)$ increases by 0.1 Å, *i.e.*, simulating the base-pair stretching upon collisional activation. An energy barrier for intra-base pair PT emerges on this slice, as indicated by the yellow star at $PE = 0.85$ eV. Accompanying with the emergence of the PT barrier is the evolution of a second local minimum at $r(N7–H)=1.05$ Å, indicating the formation of an excited $(9MOG^{\bullet+} \cdot 9MA)^{*}$ structure. Interestingly, the PT barrier height keeps increasing with the increasing $r(N1'–H)$, as illustrated by the yellow trajectory in FIG. 4(b). The barrier is 1.09 eV at $r(N7–N1') = 3.0$ Å, and rises to 1.97 eV at 3.3 Å and 2.9 eV at 3.6 Å. The implications are two-fold: first, PT becomes feasible as soon as the base pair is activated and stretching from an equilibrium distance; secondly, once $r(N7–N1')$ stretches to exceeding 3.3 Å, the PT barrier increases to beyond 1.97 eV and can no longer compete with the di-

rect dissociation of $[9MOG–H_{N7}]^{\bullet}\cdot[9MA+H_{N1'}]^{+} \rightarrow$ $[9MOG - H_{N7}]^{\bullet} + [9MA+H_{N1'}]^{+}$ (which opens at 1.8 eV). It is reasonable to assume that, at high E_{CM}, the r(N7−N1') bond is stretching much quickly, and it is only a short time duration for the PT barrier to increase beyond 1.8 eV. This may explain that the cross section for $[9MOG - H_{N7}]^{\bullet}\cdot[9MA+H_{N1'}]^{+} \xrightarrow{PT}$ $9MOG^{\bullet+}\cdot9MA \xrightarrow{\text{dissociation}} 9MOG^{\bullet+} + 9MA$ stops increasing at $E_{CM} = 2.2$ eV and decreases quickly starting at 3.8 eV; and most of all, this product channel remains minor throughout the whole E_{CM} range.

This ion-beam experiment was not designed to distinguish different base-pair conformers of similar energies. To determine whether $[9MOG - H_{N7}]^{\bullet}\cdot[9MA+H_{N1'}]^{+}\_B$ would be able to produce a similar double-well potential to promote PT upon collisional activation, another set of relaxed 2D PES scan was carried out for this conformer. The results are shown in FIG. S1 (SM). The two sets of PESs in FIG. 4 and FIG. S1 have produced nearly identical features upon base-pair stretching/separation, emphasizing the generality of the double-well PES for different $[9MOG\cdot9MA]^{\bullet+}$ conformers.

V. CONCLUSION

A guided-ion beam study was carried out to examine the collisional activation dynamics and products of $[9MOG\cdot9MA]^{\bullet+}$. The $[9MOG\cdot9MA]^{\bullet+}$ reactant ion beam consisted of solely intra-base pair proton-transferred, Hoogsteen-type $[9MOG - H]^{\bullet}\cdot[9MA+H]^{+}$ conformers. On the other hand, the measurement of kinetic energy-dependent CID revealed two pairs of dissociation products: the pair of $9MOG^{\bullet+} + 9MA$ with the 0 K dissociation threshold of 1.65 ± 0.1 eV, which was expected only from a $9MOG^{\bullet+}\cdot9MA$ precursor; and the pair of $[9MOG - H]^{\bullet} + [9MA+H]^{+}$ with the 0 K dissociation threshold of 1.8 ± 0.1 eV, which was expected only from a $[9MOG - H]^{\bullet}\cdot[9MA+ H]^{+}$ precursor. To explore the dissociation mechanism, reaction PESs were mapped out for two major $[9MOG - H]^{\bullet}\cdot[9MA+H]^{+}$ conformers. Both base-pair conformers could form an activated $(9MOG^{\bullet+}\cdot9MA)^{*}$ intermediate through intra-base pair PT upon collisional activation, and the $(9MOG^{\bullet+}\cdot9MA)^{*}$ intermediate provided a convenient pathway leading to $9MOG^{\bullet+} + 9MA$. The product branching of $9MOG^{\bullet+} + 9MA$ remained as minor throughout the CID experiment and decreased at colli-

sion energies above 4 eV. This observation may be correlated with the theoretical prediction that the PT barrier for $([9MOG - H]^{\bullet}\cdot[9MA+H]^{+})^{*} \rightleftharpoons (9MOG^{\bullet+}\cdot9MA)^{*}$ increases more quickly at higher energy activation, rendering the PT from $([9MOG - H]^{\bullet}\cdot[9MA+H]^{+})^{*}$ to $(9MOG^{\bullet+}\cdot9MA)^{*}$ being less competitive with the direct dissociation of $([9MOG - H]^{\bullet}\cdot[9MA+H]^{+})^{*}$. This work has explored the less intuitive aspects of purine–purine base-pair interactions and opening, and is biologically important considering the OG·A opening is a prerequisite for introducing the G·C→T·A mutation in replication and transcription [68].

Supplementary materials: Hydrogen-transferred conformers (Scheme S1) and 2D PES for $[9MOG–H_{N7}]^{\bullet}\cdot[9MA+H_{N1'}]^{+}\_B$ (FIG. S1), and Cartesian coordinates of all calculated structures are shown.

VI. ACKNOWLEDGEMENTS

[1] J. Zhou, O. Kostko, C. Nicolas, X. Tang, L. Belau, M. S. de Vries, and M. Ahmed, J. Phys. Chem. A **113**, 4829 (2009).

[2] M. Schwell and M. Hochlaf, Top. Curr. Chem. **355**, 155 (2015).

[3] S. Steenken and S. V. Jovanovic, J. Am. Chem. Soc. **119**, 617 (1997).

[4] C. J. Burrows and J. G. Müller, Chem. Rev. **98**, 1109 (1998).

[5] J. Cadet and P. D. Mascio, *8-Oxo-7, 8-Dihydro-2'-Deoxyguanosine: A Major DNA Oxidation Product*, Weinheim: Wiley-VCH Verlag Gmbh & Co. KGaA, (2008).

[6] A. M. Fleming and C. J. Burrows, DNA Repair **56**, 75 (2017).

[7] Y. Ye, J. G. Muller, W. Luo, C. L. Mayne, A. J. Shallop, R. A. Jones, and C. J. Burrows, J. Am. Chem. Soc. **125**, 13926 (2003).

[8] J. L. Ravanat, G. R. Martinez, M. H. G. Medeiros, P. Di Mascio, and J. Cadet, Tetrahedron **62**, 10709

(2006).

[9] Y. Ye, J. G. Muller, and C. J. Burrows, J. Org. Chem. **71**, 2181 (2006).

[10] G. R. Martinez, J. L. Ravanat, J. Cadet, M. H. Gennari de Medeiros, and P. Di Mascio, J. Mass Spectrom. **42**, 1326 (2007).

[11] S. Raoul, M. Berger, G. W. Buchko, P. C. Joshi, B. Morin, M. Weinfeld, and J. Cadet, J. Chem. Soc., Perkin Trans. **2**, 371 (1996).

[12] J. Cadet, T. Douki, D. Gasparutto, and J. L. Ravanat, Mutation Res. **531**, 5 (2003).

[13] J. Cadet, M. Berger, G. W. Buchko, P. C. Joshi, S. Raoul, and J. L. Ravanat, J. Am. Chem. Soc. **116**, 7403 (1994).

[14] S. Steenken, Chem. Rev. **89**, 503 (1989).

[15] J. Cadet and J. R. Wagner, Arch. Biochem. Biophys. **557**, 47 (2014).

[16] H. Sies, *Oxidative Stress*, London: Academic Press, (1985).

[17] S. Boiteux and J. P. Radicella, Biochimie **81**, 59 (1999).

[18] F. Prat, K. N. Houk, and C. S. Foote, J. Am. Chem. Soc. **120**, 845 (1998).

[19] S. Steenken, S. V. Jovanovic, M. Bietti, and K. Bernhard, J. Am. Chem. Soc. **122**, 2373 (2000).

[20] S. Shibutani, M. Takeshita, and A. P. Grollman, Nature **349**, 431 (1991).

[21] P. M. Gannett and T. P. Sura, Chem. Res. Toxicol. **6**, 690 (1993).

[22] G. W. Hsu, M. Ober, T. Carell, and L. S. Beese, Nature **431**, 217 (2004).

[23] L. G. Brieba, B. F. Eichman, R. J. Kokoska, S. Doublié, T. A. Kunkel, and T. Ellenberger, EMBO J. **23**, 3452 (2004).

[24] W. A. Beard, V. K. Batra, and S. H. Wilson, Mutat. Res. Genet. Toxicol. Environ. Mutagen. **703**, 18 (2010).

[25] V. K. Batra, D. D. Shock, W. A. Beard, C. E. McKenna, and S. H. Wilson, Proc. Natl. Acad. Sci. USA **109**, 113 (2012).

[26] J. Reynisson and S. Steenken, J. Mol. Struct.: Theochem **723**, 29 (2005).

[27] S. J. Culp, B. P. Cho, F. F. Kadlubar, and F. E. Evans, Chem. Res. Toxicol. **2**, 416 (1989).

[28] K. E. McAuley-Hecht, G. A. Leonard, N. J. Gibson, J. B. Thomson, W. P. Watson, W. N. Hunter, and T. Brown, Biochemistry **33**, 10266 (1994).

[29] S. Kumar, B. J. Lamarche, and M. D. Tsai, Biochemistry **46**, 3814 (2007).

[30] A. Irimia, R. L. Eoff, F. P. Guengerich, and M. Egli, J. Biol. Chem. **284**, 22467 (2009).

[31] K. N. Kirouac and H. Ling, Proc. Natl. Acad. Sci. USA **108**, 3210 (2011).

[32] E. D. Larson, K. Iams, and J. T. Drummond, DNA Repair **2**, 1199 (2003).

[33] S. D. Bruner, D. P. G. Norman, and G. L. Verdine, Nature **403**, 859 (2000).

[34] M. Hollstein, B. Shomer, M. Greenblatt, T. Soussi, E. Hovig, R. Montesano, and C. C. Harris, Nucleic Acids Res. **24**, 141 (1996).

[35] A. M. Fleming, J. G. Muller, A. C. Dlouhy, and C. J. Burrows, J. Am. Chem. Soc. **134**, 15091 (2012).

[36] P. O. Löwdin, Rev. Mod. Phys. **35**, 724 (1963).

[37] K. Kawai, Y. Osakada, and T. Majima, ChemPhysChem **10**, 1766 (2009).

[38] Y. Fang and J. Liu, J. Phys. Chem. A **113**, 11250 (2009).

[39] L. Feketeová, E. Yuriev, J. D. Orbell, G. N. Khairallah, and R. A. J. O'Hair, Int. J. Mass Spectrom. **304**, 74 (2011).

[40] P. Cheng and D. K. Bohme, J. Phys. Chem. B **111**, 11075 (2007).

[41] Y. Sun, M. M. Moe, and J. Liu, Phys. Chem. Chem. Phys. **22**, 14875 (2020).

[42] M. M. Moe, J. Benny, and J. Liu, Phys. Chem. Chem. Phys. **24**, 9263 (2022).

[43] M. M. Moe, M. Tsai, and J. Liu, ChemPhysChem **24**, e202300511 (2023).

[44] R. K. O. Sigel, E. Freisinger, and B. Lippert, J. Biol. Inorg. Chem. **5**, 287 (2000).

[45] K. M. Ervin and P. B. Armentrout, J. Chem. Phys. **83**, 166 (1985).

[46] P. B. Armentrout, Int. J. Mass Spectrom. **200**, 219 (2000).

[47] P. B. Armentrout, J. Anal. At. Spectrom. **19**, 571 (2004).

[48] C. Rebick and R. D. Levine, J. Chem. Phys. **58**, 3942 (1973).

[49] R. D. Levine and R. B. Bernstein, *Molecular Reaction Dynamics and Chemical Reactivity*, New York: Oxford University Press, (1987).

[50] J. Liu, B. van Devener, and S. L. Anderson, J. Chem. Phys. **116**, 5530 (2002).

[51] M. M. Moe, J. Benny, Y. Sun, and J. Liu, Phys. Chem. Chem. Phys. **23**, 9365 (2021).

[52] P. J. Chantry, J. Chem. Phys. **55**, 2746 (1971).

[53] C. Lifshitz, R. L. C. Wu, T. O. Tiernan, and D. T. Terwilliger, J. Chem. Phys. **68**, 247 (1978).

[54] M. B. Sowa-Resat, P. A. Hintz, and S. L. Anderson, J. Phys. Chem. **99**, 10736 (1995).

[55] M. T. Rodgers, K. M. Ervin, and P. B. Armentrout, J. Chem. Phys. **106**, 4499 (1997).

[56] R. A. Marcus, J. Chem. Phys. **20**, 359 (1952).

[57] M. J. Frisch, G. W. Trucks, H. B. Schlegel, G. E. Scuseria, M. A. Robb, J. R. Cheeseman, G. Scalmani, V. Barone, G. A. Petersson, H. Nakatsuji, X. Li, M. Caricato, A. V. Marenich, J. Bloino, B. G. Janesko, R. Gomperts, B. Mennucci, H. P. Hratchian, J. V. Ortiz, A. F. Izmaylov, J. L. Sonnenberg, D. Williams-Young, F. Ding, F. Lipparini, F. Egidi, J. Goings, B.

02 June 2024 19:27:07

Peng, A. Petrone, T. Henderson, D. Ranasinghe, V. G. Zakrzewski, J. Gao, N. Rega, G. Zheng, W. Liang, M. Hada, M. Ehara, K. Toyota, R. Fukuda, J. Hasegawa, M. Ishida, T. Nakajima, Y. Honda, O. Kitao, H. Nakai, T. Vreven, K. Throssell, J. A. Montgomery Jr. , J. E. Peralta, F. Ogliaro, M. J. Bearpark, J. J. Heyd, E. N. Brothers, K. N. Kudin, V. N. Staroverov, T. A. Keith, R. Kobayashi, J. Normand, K. Raghavachari, A. P. Rendell, J. C. Burant, S. S. Iyengar, J. Tomasi, M. Cossi, J. M. Millam, M. Klene, C. Adamo, R. Cammi, J. W. Ochterski, R. L. Martin, K. Morokuma, O. Farkas, J. B. Foresman, and D. J. Fox, *Gaussian 16*, Wallingford, CT: Gaussian Inc., (2016).

[58] A. Kumar and M. D. Sevilla, J. Phys. Chem. B **118**, 5453 (2014).

[59] I. M. Alecu, J. Zheng, Y. Zhao, and D. G. Truhlar, J. Chem. Theory Comput. **6**, 2872 (2010).

[60] F. B. van Duijneveldt, J. G. C. M. van Duijneveldt-van de Rijdt, and J. H. van Lenthe, Chem. Rev. **94**, 1873 (1994).

[61] Y. Sun, M. M. Moe, and J. Liu, Phys. Chem. Chem. Phys. **22**, 24986 (2020).

[62] W. Lu and J. Liu, Phys. Chem. Chem. Phys. **18**, 32222 (2016).

[63] S. Wei, Z. Zhang, S. Liu, and Y. Wang, New J. Chem. **45**, 11202 (2021).

[64] G. Kampf, L. E. Kapinos, R. Griesser, B. Lippert, and H. Sigel, J. Chem. Soc., Perkin Trans. **2**, 1320 (2002).

[65] T. R. Harkins and H. Freiser, J. Am. Chem. Soc. **80**, 1132 (1958).

[66] C. Larriba and C. J. Hogan Jr., J. Comput. Phys. **251**, 344 (2013).

[67] C. Larriba-Andaluz and C. J. Hogan Jr., J. Chem. Phys. **141**, 194107 (2014).

[68] U. Dornberger, M. Leijon, and H. Fritzsche, J. Biol. Chem. **274**, 6957 (1999).

02 June 2024 19:27:07